RSC Advances

ROYAL SOCIETY OF CHEMISTRY

www.rsc.org/advances

Amorphous Carbon Nanotubes as Potent Sorbents for Removal of Phenolic Derivative Compound and Arsenic: Theoretical Support of Experimental Findings

P. Bhowmik[1)], D. Banerjee[1*#)], S. Santra[2)], D. Sen[2)], B. Das[1)], K. K. Chattopadhyay[1,2,*)]

[1)]School of Material Science and Nanotechnology
[2)]Thin Film and NanoScience Laboratory, Department of Physics,
Jadavpur University, Kolkata 700032, India
[#]Present Address: Academy of Technology G.T. Road (Adisaptagram) Aedconagar
Hooghly-712121; India.

Abstract:

This work depicts the adsorptive removal efficiency of carcinogenic phenolic derivative compound, Resorcinol and highly toxic Arsenic (III) from water by low temperature, chemically synthesized amorphous carbon nanotubes (a-CNTs). The as prepared a-CNTs were characterized by X-ray diffraction, field emission scanning electron microscopy (FESEM), high resolution transmission electron microscopy; Raman spectroscopy and Fourier transform infrared spectroscopy.

The a-CNTs were used in order to remove both organic pollutant as well as heavy metal like Arsenic (III) by the process of adsorption. The quantification has been made with the help of UV-Vis Spectroscopy. The removal efficiency of a-CNTs for both Resorcinol and Arsenic (III) was analysed by kinetic spectrophotometric study. It is seen that for Resorcinol, the maximum possible removal efficiency was 76 % within a time period of about 5 hours. Several sorption parameters like contact time, adsorbent dosage and pH were inspected for adsorption of Resorcinol. For Arsenic (III), the removal efficiency was 42%. Also first principle study has been done and the adsorption of As adatoms on 5-8-5 type double vacancy defects is computationally investigated as a simplified case for As(III) atom trapping by a-CNTs. It is seen that native point defects of a-CNTs bonds strongly with As adatoms.

***Corresponding author**: kalyan_chattopadhyay@yahoo.com (K. K. Chattopadhyay)
nilju82@gmail.com (D. Banerjee)

1. Introduction:

Recently, water pollution has been a burning issue owing to hastily growing industrialisation and urbanisation. Phenolic derivatives as industrial raw materials or intermediates are quite indispensable in several industries like food additives, hair dyes, dyes, plastics, synthetic fibres, textile, paper, pulp, steel, petrochemical, petroleum refinery, rubber, dye, plastic, pharmaceutical, cosmetics, insecticides, weed killers, etc. However, excessive use of these, cause environmental hazards and severe human health problems.

Again, the ensuing concern is arsenic contamination of water. This has perturbed various parts of the world including North America and Asia [1-3]. Apart from being classified as a Group 1 carcinogen [4], it's the cause behind several serious health hazards including spontaneous abortion [5]. The US-EPA maximum contaminant level for arsenic was reduced from 50 to 10 ppb in 2001. In an aquatic ecosystem arsenic is predominant in two different oxidation states. Arsenite or As (III) and Arsenate or As(V) of which As (III) is more toxic and more difficult to remove from aquatic systems as compared to As(V) [6].

Several approaches have been adapted for the remediation/degradation of organic pollutants like phenolic derivatives and inorganic toxic pollutant like arsenic. The conventional methods include biodegradation anaerobic biodegradation, anodic oxidation, photo-catalysis, oxidative catalysis, precipitation, coagulation, nanofiltration, reverse osmosis. Electrodialysis, adsorption, ion exchange, foam floatation, solvent extraction, etc. Of which adsorption techniques have gained favour due to their efficacy and simplicity regarding removal of both organic as well as inorganic pollutants. Use of ZORBAXSPE C_{18} cartridge, activated carbon, granular activated carbon, etc for extraction of phenolic compounds [7] and use of polymeric resins, activated carbon, activated alumina, iron oxides and natural ores [8] have aroused high interest for a superior adsorbent with superior performance. Long and Yang [9] first reported that CNTs could act as superior adsorbents for dioxin and the removal capacity of CNTs was

found to be much higher than that of activated carbon. It was also found that CNTs could be used as efficient adsorbents in a wide pH range of 3-10 [10, 11].

Since its very inception in 1991 by Iijima [12], carbon nanotubes (CNTs) have enthralled researchers from umpteen genres due to their neoteric chemical and physical properties. The extraordinary features of CNTs like high aspect ratio; relatively large specific surface area (SSA); excellent mechanical, electrical and thermal properties, endow them with the credit of becoming a suitable candidate for a plethora of applications such as probes, sensors, lithium batteries, gas adsorption as well as hydrogen storage [13]. CNTs also exhibit phenomenal sorption properties towards various organic compounds and inorganic ions [14]. The potential for sidewall functionalization and surface modification make them tempting as support phases for wastewater treatment [15-17].

However, the maximum of related studies have been done on crystalline CNTs which suffer from its inherent drawbacks like very low yield, very critical deposition conditions like the requirement of high operating temperature, catalyst support, long synthesis period, expensive production costs, and complex processing steps [18]. These challenges prompted researchers to develop simpler synthesis routes for synthesizing novel CNTs in a large scale. In that light, amorphous carbon nanotubes (a-CNTs) have turned out to be low cost alternatives due to its ease of synthesis in large quantities [19]. Moreover, a-CNTs have also stirred immense interest due to their defects at the amorphous wall, more dangling bonds and larger surface area than sp^2 graphite, indicating their high efficacy in myriads of fields.

All the above studies easily reveal that a-CNTs can be good, cheap adsorbent alternatives for the remediation of water pollutants of organic as well as inorganic genre. Therefore, in the present work, Resorcinol (a phenolic derivative with hydroxyl groups in ortho and meta positions) and Arsenic (As [III]) have been selected as two organic and inorganic wastewater models respectively for realising the potency of a-CNTs in the field of adsorption. The

mechanisms of adsorption have also been investigated, which may be suggestive to further studies on removal of organic-inorganic contaminants by the same adsorbent. As far as our knowledge is concerned, there have been no previous reports on adsorption of phenolic derivatives and arsenic by a-CNTs.

2. Experimental and Characterization

The a-CNTS used for adsorption of Resorcinol and Arsenic were synthesised by a low temperature assisted process described in our previous work [20], where, certain amount of ammonium chloride and ferrocene, all analytically pure grades, were taken and thoroughly mixed in a mortar for 30 minutes. The mixture was then taken in a Borosil 250 mL glass beaker. A glass petridish was kept over the beaker as a cover to avoid immediate evaporation of ferrocene when the mixture was heated. The beaker was then inserted into an air furnace maintained at 250 °C. The heating was continued for 30 minutes and the sample was allowed to cool naturally. The resultant black powder was washed consecutively by diluted HCl and deionized water to remove the presence of trace amount of iron and filtered. The black residue was finally dried for 24 hours at temperature 80 °C.

The as prepared a-CNTs were characterized by X-ray diffraction (XRD Bruker, D8 Advance). The morphology of the as prepared samples was studied by field emission scanning electron microscope (FESEM, Hitachi, S-4800) and high resolution transmission electron microscopy (HRTEM, JEOL-JEM 2100). Raman spectroscopic study were done with the help of Witec Raman spectrometer (excitation wavelength λ_{ex}= 532 nm), and FTIR (Shimadzu FTIR-8400S) analysis. Also the quantification of the removal efficiency has been obtained by UV-Vis spectroscopic (Shimadzu UV-3600) study.

Adsorbates: The adsorbates used in the experiment were of analytical grade and were obtained from Spectrochem Company and Merck, Germany respectively. The working

solution for Resorcinol was prepared by addition of 50mg Resorcinol crystals per litre of deionised water followed by 20 minutes of sonication.

The stock solution of As (III) was prepared by dissolving 0.5 ml of $NaAsO_2$ in 1 litre of deionised water.

Adsorption studies:

(a) Resorcinol: 0.5 g of the adsorbent (a-CNTS) was mixed into 150 ml of working solution with in a series of 250 ml Borosil beakers at a pH of 6-7. The mixture was sonicated for 20 minutes and stirred with the aid of magnetic stirrer for distinct time periods of 1h, 3h and 5h to ensure complete adsorption. The suspensions were filtered after stipulated time period and the filtrates were analysed using UV-Vis spectrophotometer. The amount of Resorcinol adsorbed onto a-CNTs was calculated by using the following equation [21]:

$$q_e = \left[\frac{\{(C_0 - C_e) \times V\}}{m}\right] \quad (1)$$

Where, q_e and q_t are adsorbed amounts by a-CNTs (mg/gm) at equilibrium and at time t respectively; C_0 is the initial concentration of dye (mg/ml); C_e is the equilibrium concentration of dye (mg/ml); C_t is the concentration of dye at any time *t; V* is the solution volume (ml); *m* is the a-CNTs dosage (gm).

(b) Arsenic (III): 20 ml of 0.5ml/l As (III) solution was contacted with a-CNTs ranging from .005 gm to .02 gm and the supernatant solution obtained after filtration was collected after 1h of stirring in each case. The samples were then analysed for kinetic studies by UV-Vis spectroscope.

3. Results and discussions:

3.1 Characterization of adsorbents:

XRD pattern of a-CNTs is shown inset **Fig.1** a, where the spectra has been taken by irradiating the as-prepared sample by Cu Kα radiation (λ = 0.15406 nm) operated at 40 kV,

40 mA with a normal θ - 2θ scanning. It can be clearly observed from the XRD plot that the sample has no intense peak throughout the region barring a broadened hump at around 25°; thus it can be concluded that this is amorphous in nature and this amorphousness originates from the low temperature synthesis of the sample [22].

Fig.1 shows the FESEM images of the pure a-CNTs (a-d) with different magnifications with TEM image shown in **Fig.1** e and f. It is seen that a-CNTs have been formed uniformly over a large area. The average diameters of the as prepared a-CNTs are not more than 200 nm and length several microns. The hollowness of the as synthesized 1 D structure can be clearly seen from **Fig.1** (c and d) and thus it is confirmed that the as synthesized 1 D structure is not carbon fibres but carbon nanotubes. The HRTEM images also support the same. Moreover from the SAED pattern shown inset the amorphousness of the sample can further be confirmed.

The exact growth mechanism for a-CNTs formation is hard to predict but one can follow Liu and his co-worker for their similar kind of structure [23].

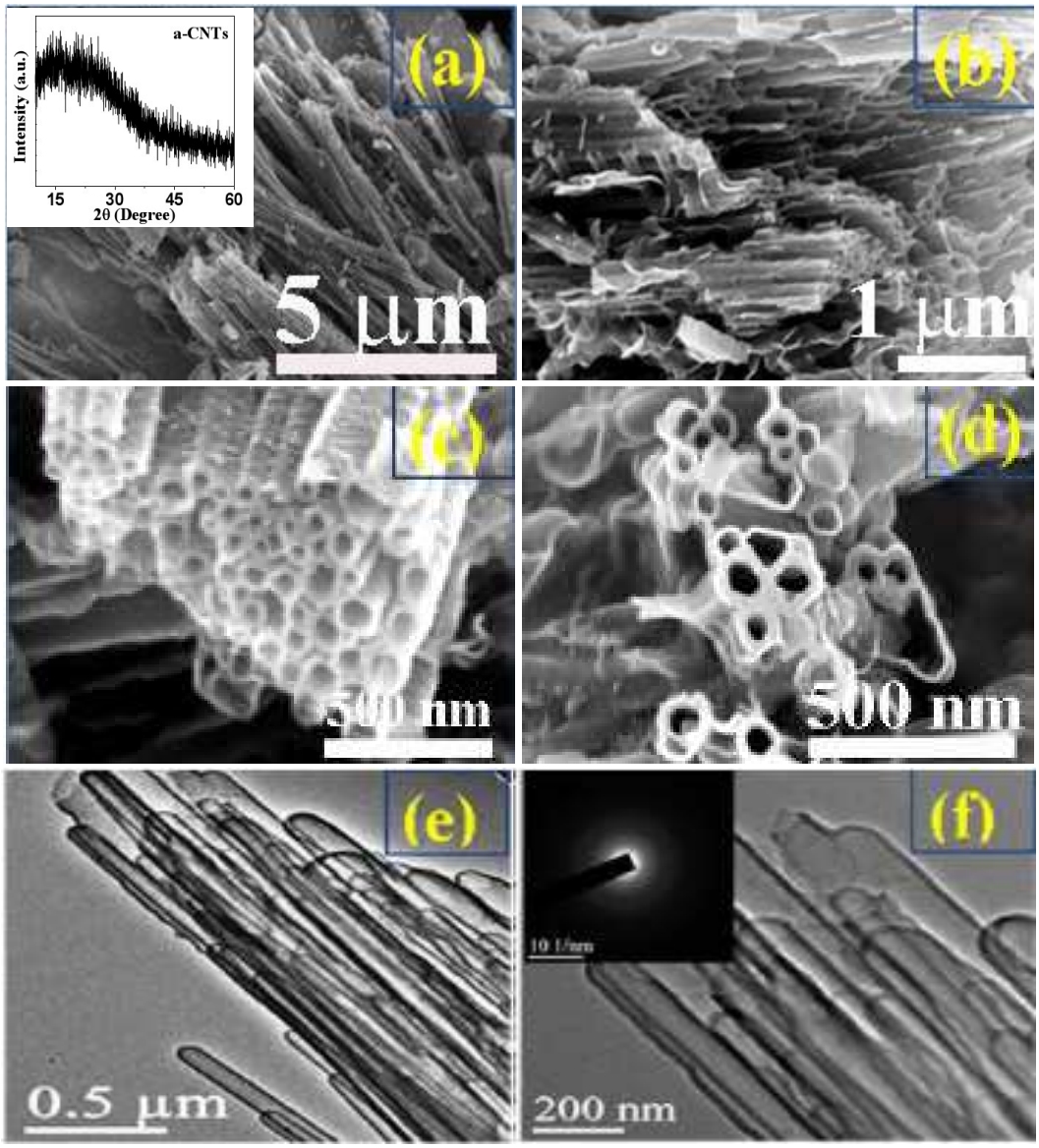

Fig.1: (a-d) FESEM and (e, f) TEM images of a-CNTs with different magnification (inset **1 a**, XRD pattern of a-CNTs and **1 f**, corresponding SAED pattern is shown).

Fig.2 (a, b) shows the Raman spectra of pure a-CNTs and that after adsorption of resorcinol. The D and G bands are discernible at ~ 1380 and at ~ 1530 cm^{-1}, respectively for pure a-CNTs. The D band is attributed to the Raman inactive A_{1g} in plane breathing vibration mode. The D band can be assigned to the vibration of the carbon atoms with dangling bonds in plane terminations of disordered graphite and thus being associated with presence of defects within the hexagonal graphitic layers. The G band is attributed to the Raman active E_{2g} in plane

vibration mode related to vibration of sp^2 bonding within the carbon atoms in a 2D hexagonal lattice such as in graphite layers [24].

It is to be noted that he intensity ratio of I_D/I_G is the measure of the corresponding parameter present in the sample. Here instead of calculating I_D/I_G ratio we have calculated the ratio of integrated areas (A_G/A_D) of these two bands by deconvoluting in origin software to determine the relative content of sp^2 hybridized carbon in ring pattern and it has come out to **be** ~ 16.49, 21.35 % for pure and resorcinol modified a-CNTs. Also Raman spectra can very effectively be used to determine sp^3 content present in the sample that can be evaluated quantitatively using the relation

$$sp^3 \text{ content} = 0.24 - 48.9 \times (\gamma_G - 0.1580) \quad (2)$$

where γ_G is the peak position of G band in inverse of micrometer unit. The value of the sp^3 content of both the samples have come out to be~ 0.31, 0.24. In **Fig.2 b** the big hump at ~ 2800 cm^{-1} is assigned to the 2D band that is basically an overtone of the D peak involving two in-plane transverse optic phonons [25]. The peak at ~2460 cm^{-1}, known as G* , is due to the inter valley double resonant Raman process similar to that of 2D band, but involving one Longitudinal and one Transverse phonons [25].

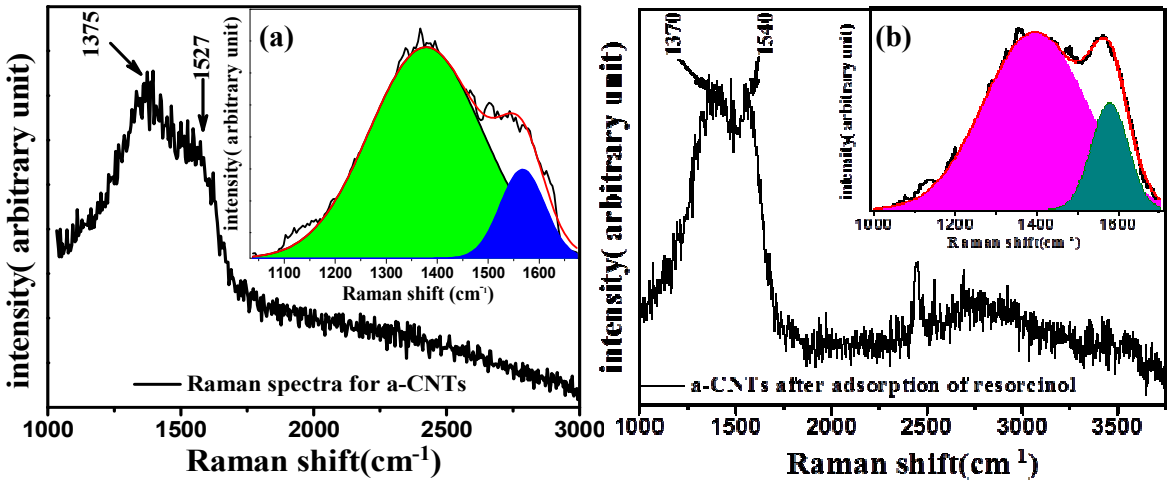

Fig.2: Raman Spectra of a-CNTs before (a) and after (b) adsorption of Resorcinol

The FTIR spectra of pure and resorcinol modified a-CNTs has been shown in **Fig.3.** One can see that there are considerable changes in the FTIR spectra of a-CNTs after adsorption of resorcinol. The peak at 627 cm^{-1} has been shifted to 654 cm^{-1} and a new peak appears at 783 cm^{-1} in case of a-CNTs after adsorption of resorcinol. Both the peaks come from the silicon wafer used as substrate for FTIR measurement [26]. The band between 1250 to 1750 cm^{-1} present in both sample are basically composed of several individual peaks as shown in the figure. Of which the peak at 1382 (or 1366) cm^{-1} comes due to the sp^3 hybridized CH_3 bond so is applicable for the peak at 1382 cm^{-1} seen in the spectra of pure a-CNTs. Peak at 1218 cm^{-1} is attributed to the sp^2/sp^3 hybridized C-C bond [27]. The peak at 1724 cm^{-1} is the signature of C=O bond present in the resorcinol modified a-CNTs. The small peak at ~ 2300 cm^{-1} is due to presence of carbon dioxide present in the atmosphere. The small band at ~ 2870 cm^{-1} in both the samples signifies the presence of $C\text{-}H_n$ bonds whereas broad band in the 2800–3500 cm^{-1} region is due to the presence of hydroxyl groups (–OH) adsorbed from atmosphere. The small peak at 3630 cm^{-1} which is not seen in case of pure a-CNTs but visible in case of other sample may be attributed to O-H stretching bond [28].

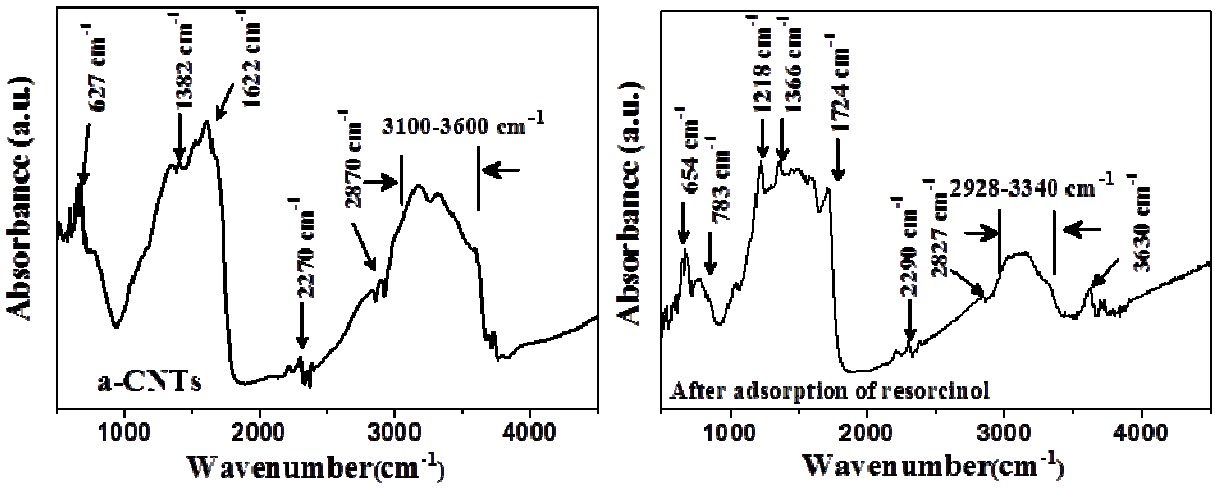

Fig.3: FTIR spectra of a-CNTs before and after adsorption of Resorcinol

3.2. Adsorption Studies:

Resorcinol: During the adsorption of resorcinol by a-CNTs, the effect of various adsorption parameters like contact time, adsorbent dosage, pH, removal efficiency, etc. have been investigated.

Effect of Contact time: Fig.4 a shows the effect of stirring time on the adsorption of resorcinol on a-CNTs. The initial concentration of resorcinol was 50 mg/L. After 1h the uptake of resorcinol was 11.53mg/L. The maximum uptake of resorcinol could be achieved at a stirring time **[t_s]** of 5h which was about 38 mg/L which is about 76% of the initial concentration. This is at par with the data shown in **Fig.4** b. This suggests that the adsorption mechanism of a-CNTs does not follow that of activated carbon or crystalline CNTs. The adsorption by activated carbon is related to the porous structure, so it takes longer time for adsorbates to diffuse through pores. In case of crystalline CNTs the most available spaces for adsorption are the cylindrical external surfaces instead of inner cavities or inner wall spacing [29]. Adsorption of resorcinol on activated carbon needs 7-20 h to reach equilibrium [30] whereas crystalline CNTs need 10 h to reach equilibrium [21].The quick adsorption of resorcinol on a-CNTs indicate that they are highly potent adsorbents compared to rest of the categories of adsorbents.

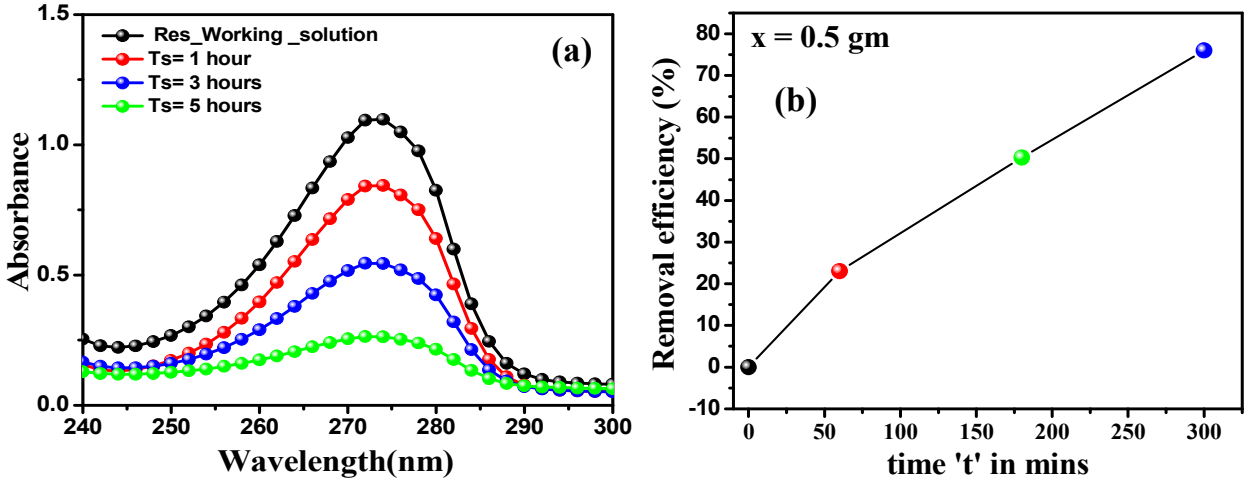

Fig.4: (a) Absorption spectra of resorcinol for different contact time and (b) corresponding variation of removal efficiency

Effect of Adsorbent dosage: Dosage amount was varied from 0.1 g to 0.5 g. The maximum adsorption efficiency could be achieved at a dosage amount of 0.5g which is evident from **Fig.5** a. The maximum uptake of resorcinol by 0.5 g of dosage was 37 mg/L which is equivalent to 74% of the initial concentration of resorcinol **Fig.5** b.

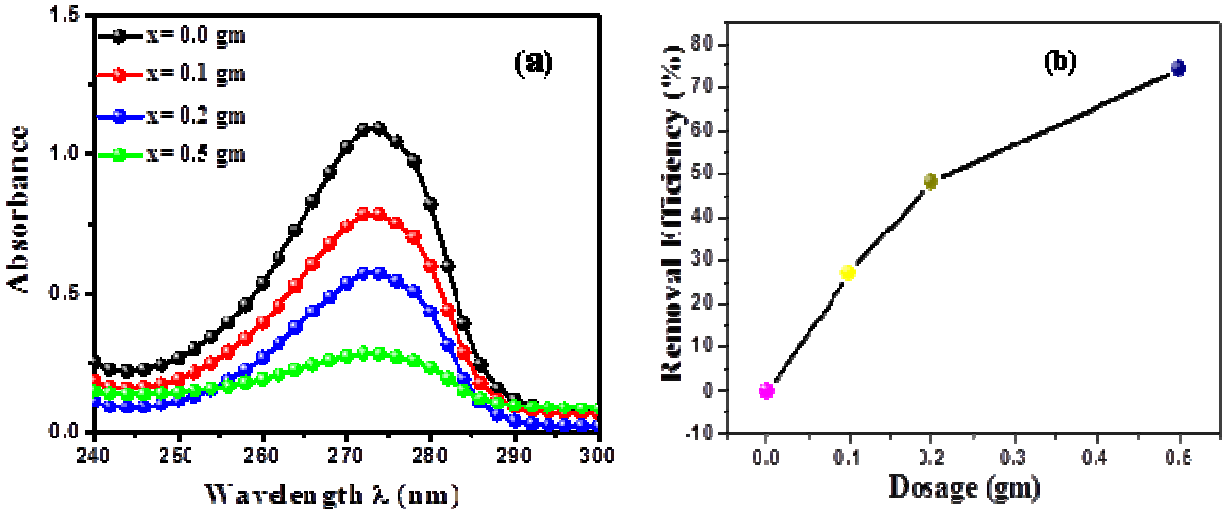

Fig.5: ((a) Absorption spectra of resorcinol for different dosage and (b) corresponding variation of removal efficiency

Effect of pH: Fig.6 shows the pH effect on the uptake of resorcinol by a-CNTs. In the pH range 8-10, Resorcinol gets oxidised due to basic condition since it has a weak acidic nature. Due to this effect solubility decreases; uptake of resorcinol increases. In the acidic condition, (pH range 1-3) hydrophilicity of a-CNTs increases. Under acidic condition a-CNT surfaces become more negatively charged [31]. As a result repulsion takes place between $C_6H_4O_2^{-2}$ (resorcinol) and CO^- (graphitic plane of a-CNTs) due to which reduction in uptake quantity takes place [32]. COOH groups on graphitic surface withdraw electrons localizing electrons from π system weakening π- π dispersion forces between aromatic ring of resorcinol and graphitic structure of a-CNTs. Hydroxyl (-OH) is an electron-donating functional group which is expected to increase the π-donating strength of the host aromatic ring. Thus, -OH is

supposed to increase the sorption affinity of resorcinol to a-CNTs graphitic surfaces through electron donor-acceptor (EDA) complex mechanism [33].

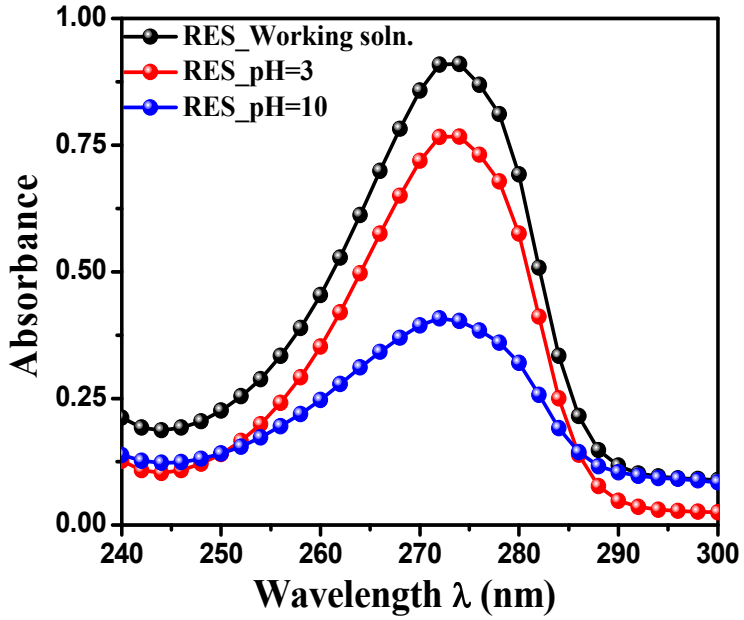

Fig.6: Effect of pH on adsorption of resorcinol

It is to be noted that Liao and his co-workers [34] reported for crystalline CNTs, the acid-treated CNTs shows poor adsorption capacity for resorcinol compared to untreated CNTs.

This is due to the fact that there are mainly four kinds of interactions that may take place between CNTs and resorcinol. These are: (a) hydrophobic interaction, (b) electrostatic attraction or repulsion, (c) hydrogen bonding between the -OH and the tube surface -OH or -COOH groups, and (d) -OH substitution enhanced π-π interactions between the phenolics and the CNTs.

This suggests that untreated CNTs are favourable for resorcinol adsorption because with increasing –COOH group the mutual electrostatic repulsion between carboxylic groups also weakening the π-π interaction and water adsorption. The location of hydroxyl group in meta-position on the aromatic ring along with its number density is another key factor that enhances the uptake of the adsorbates.

The substitution of –OH group with the hydroxy/carboxylic groups on the CNT surface may form hydrogen bonds; also there is a possibility of formation of the hydrogen bonds between the surface-adsorbed and dissolved phenolics. For crystalline CNT hydrogen bond formation may be taken to be a key factor for phenolic adsorption only at high concentration due to the fact that for crystalline CNT very low hydrogen and oxygen contents were detected suggesting lesser probability of hydrogen bonding between the phenolics and the functional groups on the CNTs. However for a-CNTs there are inherent defects onto the wall thus suggesting higher number of OH or COOH groups which is also confirmed by the FTIR spectra shown in **Fig.3**. Thus it would not be wrong if we conclude that hydrogen bonding formation is one of the major mechanisms for resorcinol adsorption.

Adsorption Kinetics: The modelling of the kinetics of adsorption of Resorcinol was investigated by two common models:

Pseudo-first-order and second order kinetic model

These models have been used several times in the past for explaining sorption mechanisms for organic as well as inorganic pollutants onto solid adsorbents (activated carbon, crystalline CNTs, etc.). The best fit model has been chosen based on the linear regression correlation coefficient values (R^2). The pseudo-first-order model can be expressed as [35]:

$$[dq_t/dt] = K_1 (q_e - q_t) \quad (3)$$

The linear form of pseudo-first-order rate equation is:

$$\ln(q_e - q_t) = \ln q_e - K_1 t \quad (4)$$

where q_e and q_t are the amounts of Resorcinol adsorbed (mg/g) at equilibrium and time t (min), respectively; K_1 is the rate constant of pseudo-first-order kinetic model (1/min). The parameters K_1 and q_e could be calculated from the slope and intercept of the plots of $\ln(q_e - q_t)$ versus t for Eq. (4). Linear form of the pseudo-second-order kinetic model can be expressed as [34]:

$$[t/ q_t]= [1/h] + [t/ q_t] \quad (5)$$

where h is given by:

$$h=K_2 q_e^2 \quad (6)$$

where K_2 (g/mg min) is the rate constant of the pseudo-second-order. The q_e and K_2 values can be obtained from the slope and intercept of plots of t/q_t versus t. **Fig.7** depicts amount of resorcinol adsorbed (q_t) with varying time (t) whereas **Fig.8** and **Fig.9** depict the linearized form of the pseudo-first-order model and pseudo-second-order model for a-CNTs' adsorption capacity at 50 mg/L initial concentration of Resorcinol. The calculated kinetics constants are given in **Table 1**. The correlation coefficients values were greater than 0.9 and the calculated q_e was approximately equivalent to the experimental value for both kinetics models, but this value for the pseudo-first-order model is much greater than pseudo-second-order model, indicating that the adsorption of Resorcinol could follow the pseudo-first-order model.

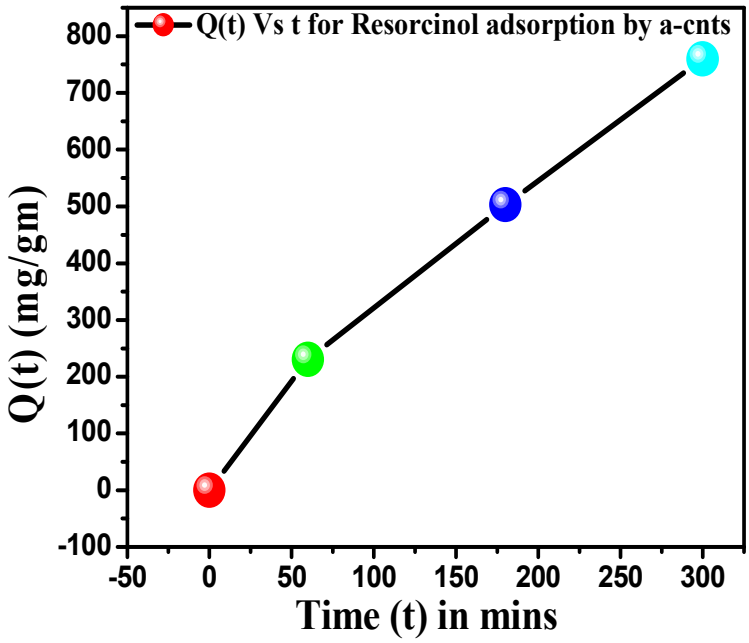

Fig.7: Effect of contact time (t) on amount of resorcinol adsorbed (q_t)

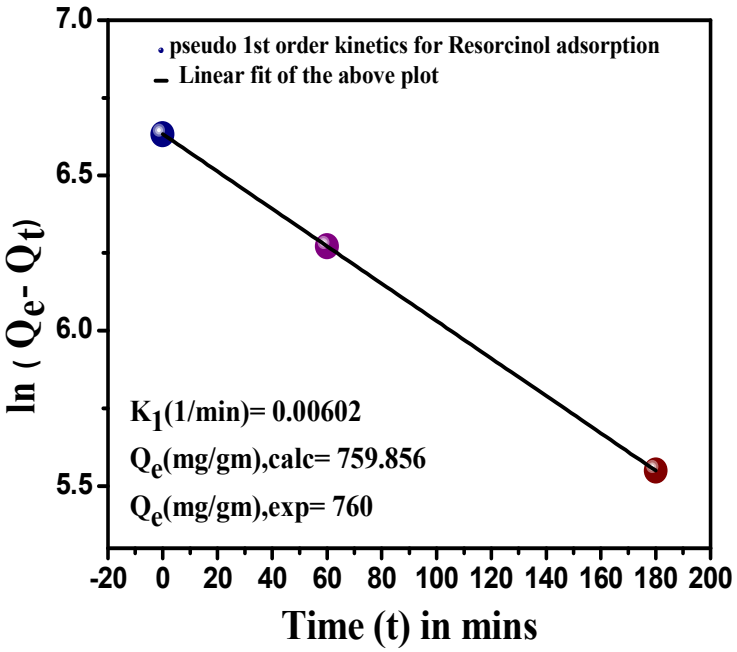

Fig.8: Linear plot of Pseudo 1st order kinetics for Resorcinol adsorption

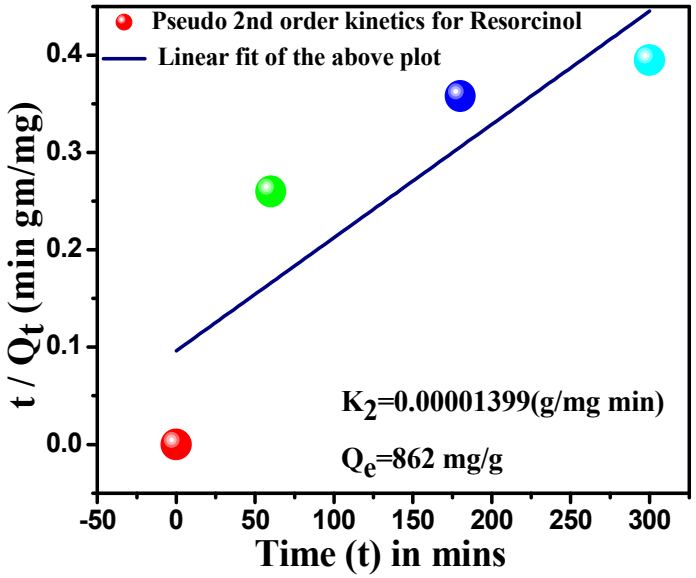

Fig.9: Linear plot of Pseudo 2nd order kinetics for Resorcinol adsorption

Table 1: Different parameters as obtained from Pseudo-1st-order and 2nd order study

Kinetic Model	Rate Constant (K)	Amount adsorbed at equilibrium q_e (gm/mg) (calculated from experiment)	Amount adsorbed at equilibrium q_e (gm/mg) (graph)	linear regression correlation coefficient value (R^2)
Pseudo-1st-order	**0.00602 min^{-1}**	**760**	**759.856**	**1**
Pseudo-2nd-order	**0.000014 gm/mg min**	**760**	**862**	**0.63**

Arsenic: Kinetic methods of analysis are quite alluring for the determination of trace amounts of arsenic as such methods have the general advantage of combining sensitivity with relatively simple procedures and apparatus [36]. Thus in this particular work of interest, the determination of As(III), by using a-CNTs as adsorbents, has been executed on the basis of its inhibitory effect on the reaction of bromate with hydrochloric acid. The method is very rapid, sensitive yet simple and has been employed previously [37] for determination of As(III) as low as 6μg L^{-1}.

Reagents for As(III) adsorption: Apart from the preparation of working solution of $NaAsO_2$, a 0.10 M potassium bromated solution was prepared by dissolving 1.67 g of $KBrO_3$ (Merck) in water and diluting to 100 ml in a borosil glass beaker. A solution of 100 mg L^{-1} methyl orange was prepared by dissolving 0.01 g of methyl orange (Merck) in water and diluting to 100 ml with water. Hydrochloric acid solution was prepared by appropriate dilution of concentrated hydrochloric acid [38].

Instrument for adsorption study: Absorbance Vs time graphs at fixed wavelength were recorded using Shimadzu model UV-3600 UV-Visible Spectrophotometer.

Recording procedure: The inhibited reaction was followed spectro-photometrically by monitoring the change in absorbance at 525 nm. A suitable amount of the filtrate solution was

transferred to a10 ml beaker, then 1.4 ml of 2.50M HCl solution was added followed by 1 ml of 100 mg l^{-1} methyl orange solution. The solution was diluted to 9 ml with water and then 1.0 ml of 4.2 x 10^{-4} M bromated solution was added. The stopwatch was started just after the addition of the bromated solution. The solution was diluted to the mark with water and a portion was transferred to the quartz cuvette within 60 seconds for measurement of the variation in absorbance with time at 525 nm.

Results and discussion: Bromate is reduced by chloride ion in acidic media to produce Br_2 and Cl_2 [36].

$$\mathbf{2BrO_3^- + 10Cl^- + 12H^+ \rightleftharpoons Br_2 + 5Cl_2 + 6H_2O} \quad (7)$$

The produced Br_2 and Cl_2 react with methyl orange and decolourize it [39].

Therefore, this reaction could be monitored spectro-photometrically by measuring the decrease in absorbance versus time at 525 nm.

The presence of As(III) in the medium slows the reaction, which is fairly fast in its absence or when the medium is acidic. As(III) reacts with the liberated Br_2 and Cl_2 according to the following reaction and causes an induction period [40]:

$$\mathbf{As(III) + X_2 \rightarrow As(V) + X^- (X= Cl \text{ or } Br)} \quad (8)$$

Fig.10 depicts the graph of absorbance change versus time for variation in adsorbent dosage (a-CNTS). The graph in **Fig.10** reveals that an increase in adsorbent dosage decreases the induction period of the reaction. It can be inferred that the liberated halogen (X) bleaches the orange colour of methyl orange with gradual increase in time. So, it can be said that the decrease in absorbance is directly proportional to amount of As (III) adsorbed by a-CNTs. The bleaching of methyl orange with liberated bromine is actually used to determine the reaction time.

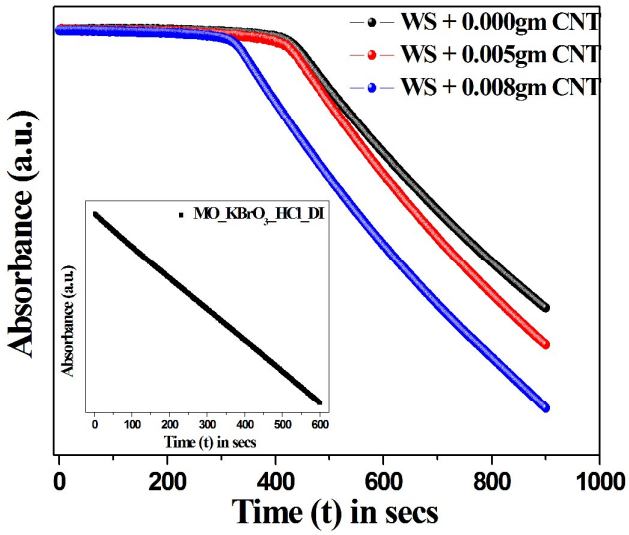

Fig.10: Absorbance versus Time plot for As (III) adsorption with varying dosage of a-CNTs; inset graph for depicting un-inhibitory reaction

Previously the inhibitory effect of As(III) under varying working conditions such as concentration variation of As(III), HCl, Methyl orange, Bromate solution and temperature variation have been reported [38], but kinetic spectro-photometric analysis of As(III) by varying doses of a-CNTs (present work) has not yet been reported. For determining the optimum amount of dosage, the absorbance change for the uninhibited reaction (reaction in the absence of arsenic) has been also executed which is evident from the inset graph provided in **Fig.10**. The removal efficiency of a-CNTs, in case of As (III) as the adsorbate, has been depicted in the form of a pie-chart, evident from **Fig.11** (where x_1, x_2, x_3 stands for working solution with 0, 0.005 and 0.008 gm. a-CNTs respectively)**.**

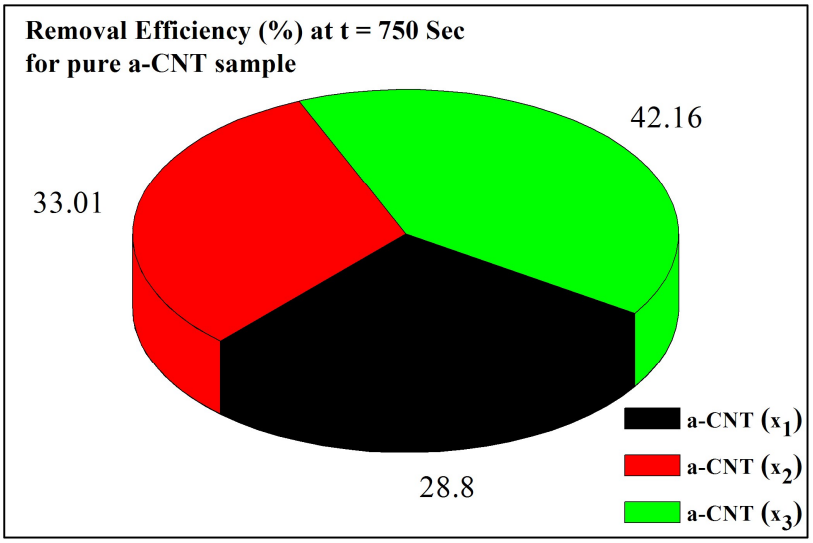

Fig.11: Removal efficiency of a-CNTs for As(III) with dose variation

Theoretical Study:

To probe the nature of the interactions between arsenic atom(s) and a-CNTs, extensive first principles calculations were carried out using plane wave basis and in both pseudopotential (PP, as implemented in CASTEP [41] code) method and projector augmented wave (PAW [42], as implemented in VASP [43-46] code) method. GGA-PBE [47] functional was used to account for the exchange and correlation effects. Plane wave cut off of 500 eV and a ~0.5/Å **k**-point grid were used in all calculations. For a robust prediction, the extents of van der Waals interactions were investigated using two separate approaches (a) empirical forcefield based PBE+D2 (Grimme's) [48] method and (b) using true first principles van der Waals density functional revPBE-vdW [49]**.** All computations were carried out in spin unrestricted manner.

As a-CNTs can be assumed to be composed of rolling of defected graphene sheets or amorphous graphene thus for adsorption purposes, fully reconstructed 5-8-5 type double vacancy defect graphene sheets (containing two pentagons and one octagon) were constructed by removal of 2 adjacent C atoms from a 72 atom, 6×6×1 graphene supercell followed by subsequent optimization. A 20 Å vacuum slab along z direction was used in all

models to ensure that no spurious interaction between the adjacent layers occurs. The adsorption energies for various As adatom adsorption configurations were quantitatively estimated using the following relation: $E_{ads} = E_{tot} - E_{far}$; where E_{ads} is the adsorption energy, E_{tot} is the total energy of the As adsorbed host and E_{far} is the total energy of the host and the As adsorbate when they are in a non-bonding configuration (~10 Å far). While using this relation, lower adsorption energies signifies stronger

It is noteworthy that, atomic structure of amorphous graphene deviates significantly from pristine graphene lattice due to the presence of large number of surface irregularities such as intrinsic/ extrinsic defects etc. and thus is computationally highly demanding to model. However the problem could be simplified by considering the interactions of As adatoms with isolated native point defects of graphene surface as a limiting case. Among various types of native point defects observed in graphene, equilibrium concentration of double vacancy (DV) defects are quite high within the typical experimental temperature range of ~1000° C [50] due to (a) high formation energies of Stone-Wales (SW) defects [51] and (b) surface migration of single vacancy (SV) defects which tend to migrate and coalesce into DVs [50, 51]. Thus in the present work, a commonly observed DV defect - DV(5-8-5), containing an octagonal and two pentagonal carbon rings, was chosen as anchoring site for As adsorption.

Graphene surface intuitively offers three plausible highly symmetric sites for adsorption: directly on the top of a C atom, over a C-C bridge and over the hollow site of a C hexagon. However not all of these sites present equal suitability towards As adatom adsorption. Earlier works [52] reported, when an As adatom is placed on the top of a C atom or over the hollow site of a C-C hexagon, it migrates away to the top of the nearest C-C bridge and bonds with two C atoms. The presence of octagonal and pentagonal rings in DV(5-8-5) complicates this scenario even more as in this case there are several different possible bridge sites, namely between hexagon (6-6) pair, octagon-pentagon (8-5), octagon-hexagon (8-6), pentagon-

hexagon (5-6) etc. Our calculations revealed the 8-5 bridge to be most favorable site for single As adatom adsorption (~0.6 eV lower adsorption energy than 6-6 bridge using PP) and this configuration (henceforth designated as: $As_{8\text{-}5}$-DV(5-8-5)) is shown in **Fig.12**. PP and PAW methods yielded comparable adsorption energies (-0.480 eV vs -0.602 eV respectively) and As-C bond lengths (2.074 Å vs 2.097 Å respectively) for this configuration. Accounting for van der Waals interactions by the means of empirical PBE+D2 (Grimme's) approach (along with PAW-PBE) did not produce any noticeable perturbation in the geometry of the $As_{8\text{-}5}$-DV(5-8-5) configuration, however a higher As adsorption energy of -0.818 eV was obtained in this case. It is to be noted that, in all of the above three cases, the nearest 2 C atoms of the adsorbate As atom was found to lift up by ~0.37 Å from the graphene plane, implying strong As-C interaction. Values of adsorption energies, optimized As-C bond lengths and vertical lift of C atoms, calculated using various methods are listed in Table 2. Optimizing $As_{8\text{-}5}$-DV(5-8-5) configuration with revPBE-vdW reveals some interesting results. In this case the adsorption energy and the As-C bond length were found to be much higher (-1.601 eV and 2.156 Å respectively), but instead of the aforementioned localized "puckering" at the adsorption location, the whole underlying adsorbent surface was found to ripple slightly (shown in **Fig.12** inset) as a consequence of As trapping. Nevertheless, the computed results imply that, in a practical scenario, binding of As adsorbate on amorphous graphene host is likely to be strongly assisted by dispersive forces.

The (partial) charges of the As adsorbate and the host C atoms for $As_{8\text{-}5}$-DV(5-8-5) configuration was computed using Mulliken population analysis. The adsorbed As adatom and its nearest two C atoms were observed to have +0.310 |e| and -0.180 |e| charges each respectively, implying a transfer of electronic (partial) charges from As to C atoms. This can be readily explained by the fact that the electronegativity (χ) of As (χ = 2.18) is much lower

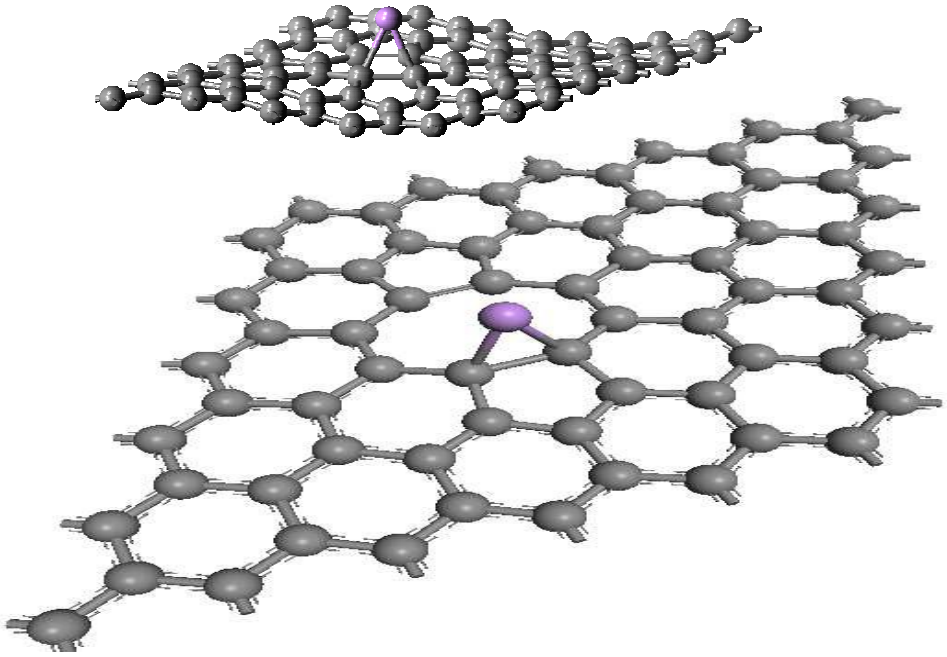

Fig.12: Optimized configuration of $As_{8\text{-}5}$-DV(5-8-5) configuration. Rippling of the underlying substrate under rev PBE-vdW is shown in inset

than that of C (χ = 2.55). As a result, the above electronic transfer renders strong ionicity to the resulting As-C bonds. The total density states (TDOS) of the $As_{8\text{-}5}$-DV (5-8-5) configuration and the projected density of states (PDOS) of the p orbitals of the As atom and its two nearest C atoms are shown in **Fig.13** and **14** respectively.

Table 2: Stability and optimized structural parameters for As adatom adsorption on 8-5 bridge of the DV(5-8-5) defect graphene: E_{ads} is the adsorption energy, l_{As-C} is the As-C bond length, Δd is the vertical lift of the two C atoms nearest to the As adatom, PP is pseudopotential method, PAW is projector augmented wave method, PBE+D2 is Grimme's empirical forcefield based vdW correction, implemented along with PAW-PBE and revPBE-vdW is first principles van der Waals density functional method based on the revised version of the PBE functional

Parameter	PP	PAW	PBE+D2	revPBE-vdW
E_{ads} (eV)	-0.480	-0.602	-0.818	-1.601
l_{As-C} (Å)	2.074	2.097	2.094	2.156
Δd (Å)	0.374	0.375	0.375	Rippling

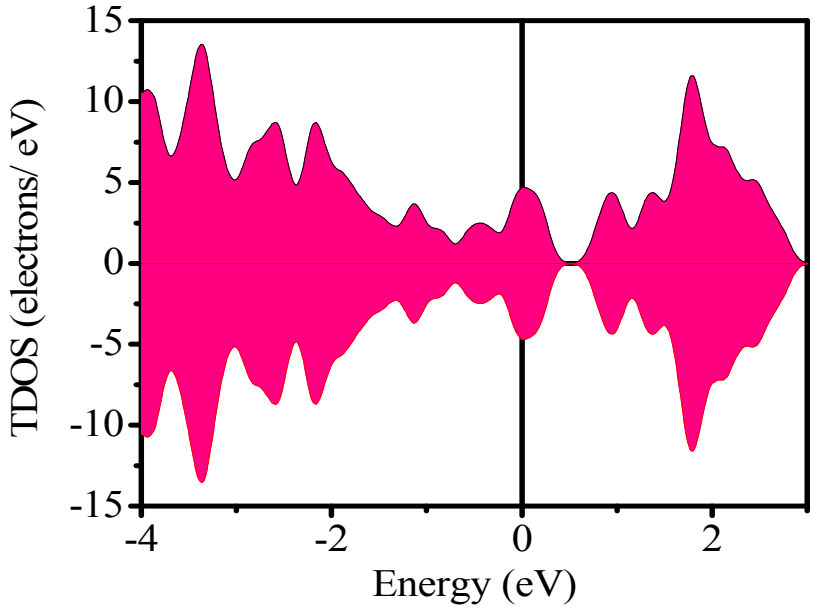

Fig.13: TDOS of As_{8-5}-DV (5-8-5) configuration

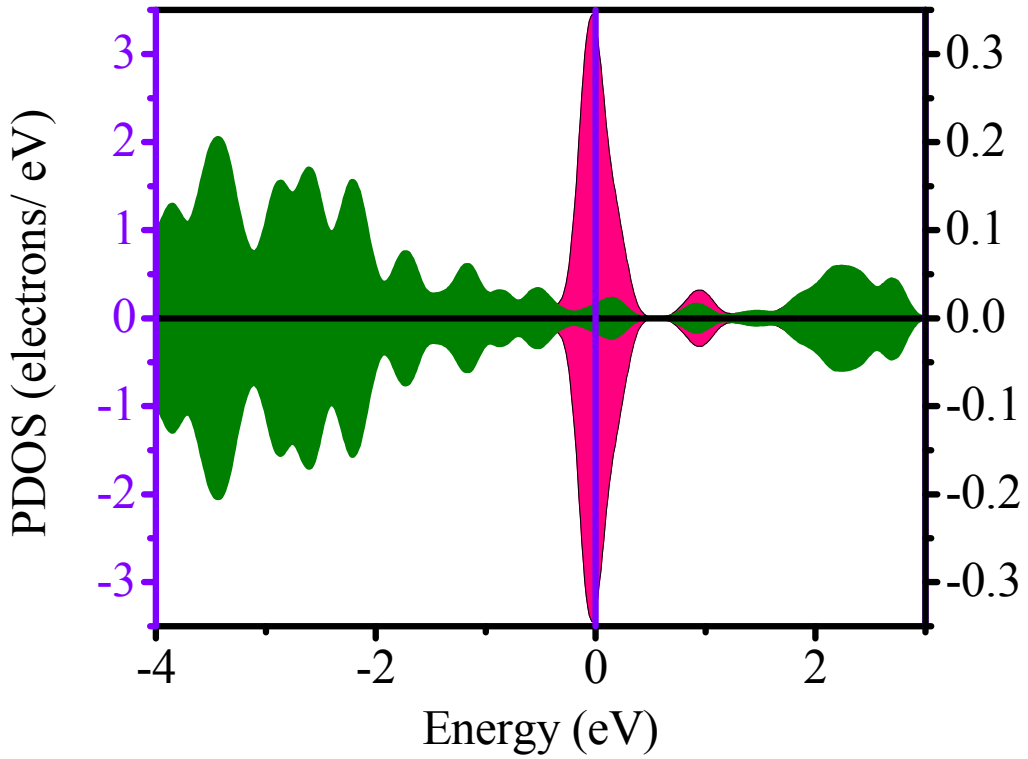

Fig.14: PDOS of As p orbitals (shown in violet) and C p orbitals (shown in green)

These two graphs clearly demonstrate that (a) $As_{8\text{-}5}$-DV(5-8-5) configuration favors a non-magnetic ground state (b) TDOS at the Fermi level is majorly dominated by As p states and (c) A small amount of orbital hybridization is present between As p states and C p states which lends minor covalency to the As-C bonds. As-C electronic interactions in $As_{8\text{-}5}$-DV(5-8-5) is graphically demonstrated in **Fig.15** by the means of electron density difference slices (red: electron enrichment, blue: electron depletion). A purely covalent bond would display electron enrichment along the bond (like the in-plane C-C bonds), however distinct electron depletion near As atom and electron enrichment near its two nearest C atoms in this case highlight the dominant ionic nature of As-C interaction.

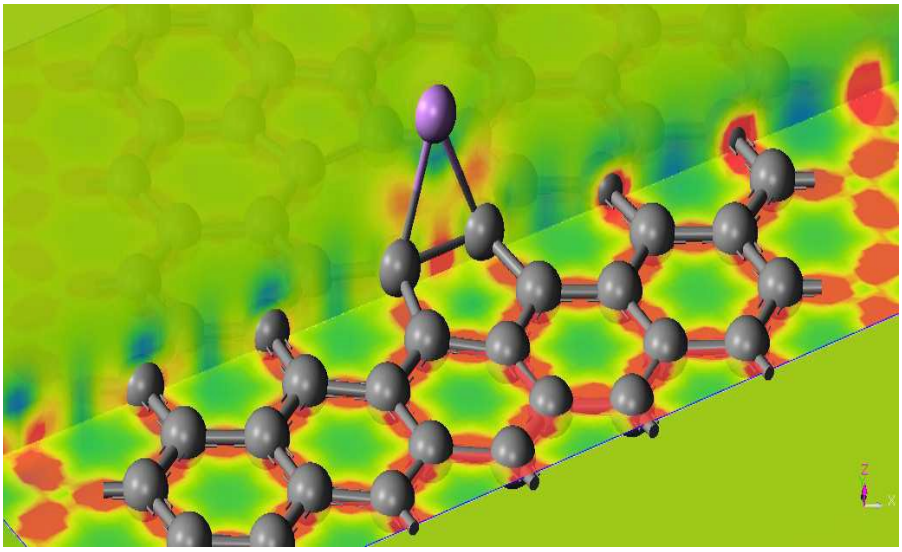

Fig.15: Electron density difference diagram for $As_{8\text{-}5}$-DV(5-8-5) configuration, scale: vertical slice (+0.15 |e| (red) to -0.15 |e| (blue); horizontal slice (+0.3 |e| (red) to -0.3 |e| (blue)).

4. Conclusion:

Amorphous CNTs (a-CNTs) has been synthesized by a very simple, low temperature solid state reaction with high yield and has been employed as a potential candidate for water purification. It has been seen that the material can be used for adsorption of hydroxyl group substituted aromatic compound like Resorcinol as well as heavy metal ion like arsenic from water.

The performance of the as synthesized material depends upon different parameters like contact time, concentration, pH of the medium etc.

Effort has been given to explain the kinetics of resorcinol adsorption with pseudo 1^{st} order or second order model.

Also from first principle study adsorption of As adatoms on 5-8-5 type double vacancy defects is computationally investigated as a simplified case for As atom trapping by amorphous graphene. It has been found that native point defects of graphene bonds strongly with As adatoms. The As-C bonding in the current model has been observed to be

predominantly ionic with minor covalency arising from overlapping of As p and C p orbitals and is greatly enhanced by contributions from vdW forces.

Acknowledgment

The authors wish to thank the University Grants Commission (UGC), the Government of India for financial support through a project and UPEII scheme and department of Science and Technology (DST), the Government of India during the execution of the work.

References:

1 M. Chetia , S. Chatterjee, S. Banerjee, M.J. Nath, L. Singh, R.B. Srivastava and H.P. Sarma, *India. Environ Monit Assess* 2011, **173,** 371–85.

2 H. Brammer and P. Ravenscroft, *Environ Int* 2009, **35**, 647–54.

3 P. Mondal, C.B. Majumder and B. Mohanty, *J. Hazard Mater*. 2006, **137,** 464– 79.

4 S.D. Richardson, *Anal Chem*. 2006, **78** 4021–45.

5 A. Navas-Acien, E.K. Silbergeld, R. Pastor-Barriuso and E. Guallar*, J. Am. Med. Assoc*. 2008, **300**, 814–22.

6 J. Pattanayak, K. Mondal, S. Mathew and S.B. Lalvani, *Carbon* 2000, **38,** 589–96.

7 Y. Cai, G. Jiang, J. Liu and Q. Zhou. *Anal Chem*. 2003, **75**, 2517– 21.

8 N.S. Addo and S. Mitra, *J. Chem. Eng. Data*. 2011, **56**, 2077–83.

9 R.Q. Long and R.T. Yang, *J. Am. Chem. Soc*. 2001, **123**, 2058–59.

10 X. Peng, Y. Li, Z. Luan, Z. Di, H. Wang, B. Tian and Z. Jia. *Chem. Phys. Lett*. 2003, **376**, 154–58.

11 S.B. Fagan, A.G.S. SouzaFilho, J.O.G. Lima, J.M. Filho, O.P. Ferreira, I.O. Mazali, O.L. Alves and M.S. Dresselhaus, *Nano Lett.* 2004, **4**, 1285–88.

12 S. Iijima, *Nature* 1991, **354**, 56–8.

13 A.C. Dillon, K.M. Jones, T.A. Bekkedahl, C.H. Kiang, D.S. Bethune and M.J. Heben, *Nature* 1997, **386,** 377–79.

14 M. Tojanowicz, *Trends Anal Chem*. 2006, **25**, 480–89.

15 Y. Wang, Z. Iqbal and S. Mitra, *Carbon* 2005, **43**, 1015–20.

16 Y. Wang, Z. Iqbal and S. Mitra, *J. Am. Chem. Soc*. 2006, **128**, 95–9.

17 S.R. Sai, Y. Chen, M.K. Kalyan, R.G. Nageswara, C. Janardhana and Mitra S. *J Nanosci Nanotechnol* 2011, **11**, 3552–59.

18 H. Nishino, R. Nishida, T. Matsui, N. Kawase and I. Mochida, *Carbon* 2003, **41**, 2819-23.

19 A. Jha, U.K. Ghorai, D. Banerjee, S. Mukherjee and K.K. Chattopadhyay, *RSC Adv*. 2013, **3**, 1227-34.

20 D. Nawn, D. Banerjee and K.K. Chattopadhyay, *Diamond Relate. Mater*. 2013, **34**, 50-59.

21 Q. Liao, J. Sun and L. Gao, *Colloids and Surfaces A* 2008, **312,** 160–65.

22 D. Banerjee, N.S. Das and K.K. Chattopadhyay, *Appl. Surf. Sci.*2012, **261**, 223–30.

23 B. Liu, D. Jia Y. Zhou, H. Feng and Q. Meng. *Carbon* 2007, **45**, 1710-13.

24 K.H. Tan and R.J. Mohd, *J. Nanopart. Res*. 2013, **15**, 1920.

25 L.M. Malard, M.A. Pimenta, G. Dresselhaus and M.S. Dresselhaus, *Physics Reports* 2009, **473**, 51-87.

26 S. Jana, S. Mondal and Bhattacharya, *J. Nanosci. Nanotechnol*. 2013, **13**, 3983-89.

27 J. Robertson, *Mater Sci. Eng. R* 2002, **37**, 129 – 281.

28 C.E. Pizzutto, J. Suave, J. Bertholdi, S.H. Pezzin, L.A.F. Coelho and S.C. Amico, *Mater. Res*. 2011, **14**, 256-63.

29 K. Yang and B. Xing, *Environ Pollut*. 2007, **145**, 529– 37.

30 A.A.M. Daifullah and B.S. Girgis, *Water Res.* 1998, **32**, 1169–77.

31 J. Chen, M.A. Hamon, H. Hu, Y. Chen, A.M. Rao, P.C. Eklund and R.C. Haddon, *Science* 1998, **282**, 95–8.

32 R.W. Coughlin and F.S. Ezra, *Environ. Sci. Technol*. 1968, **2**, 291–97.

33 M. Franz, H.A. Arafat and N.G. Pinto, *Carbon* 2000, **38**, 1807-19.

34 S. Sundaramurthy, V.C. Srivastava, I.M. Mishra, *Int. J. Energy Environ. Eng.*2012, **3**, 32 (1-19)

35 I.D. Mall, V.C. Srivastava, N.K. Agarwal and I.M. Mishra, *Chemosphere* 2005, **61**, 492-501.

36 K.B. Yatsimirskii, *Pergamon Press*, *Oxford*. 1966, **25**, xvi+ 155.

37 A. Afkhami, T. Madrakian and A.A. Assl, *Talanta* 2001, **55**, 55–60.

38 I.I. Alekseeva and L.V. Kurtova, *Zh. Anal. Khim*.1988, **43**, 1449.

39 A.E. Burgess and J.M. Ottaway, *Analyst* 1972, **97**, 357.

40 A.E. Burgess and J.M. Ottaway, *Talanta* 1975, **22**, 401-9.

41 M.D. Segall, J.D.L. Philip, M.J. Probert, C.J. Pickard, P.J. Hasnip, S.J. Clark and M.C. Payne, *J. Phys.: Condens. Matter*. 2002, **14,** 2717-44.

42 P.E. Blöchl, *Phys. Rev. B* 1994; **50**, 17953-79.

43 G. Kresse and J. Hafner, *Phys. Rev. B* 1993, **47**, 558-61.

44 G. Kresse, J. Hafner, *Phys. Rev. B* 1994, **49**, 14251-69.

45 G. Kresse and J. Furthmüller, *Comput. Mater. Sci*. 1996, **6**, 15-50.

46 G. Kresse and J. Furthmüller, *Phys. Rev. B* 1996, **54**, 11169-86.

47 J.P. Perdew, K. Burke K and M. Ernzerhof, *Phys. Rev. Lett*. 1996, **77**, 3865-68.

48 S. Grimme, *J. Comput. Chem*. 2006, **27**, 1787-99.

49 M. Dion, H. Rydberg, E. Schröder, D.C. Langreth and B.I. Lundqvist, *Phys. Rev. Lett*. 2004, **92**, 246401-4.

50 F. Banhart, J. Kotakoski and A.V. Krasheninnikov, *ACS nano* 2010, **5**, 26-41.

51 D. Sen, R. Thapa and K.K. Chattopadhyay. *Chem. Phys. Chem*. 2014, **15,** 2542-49.

52 A. Shamsu, R. Md. Mahmudur, A.Y. Zuntu, Z. Hishamuddin, M. Rifki and S. Henry, *Graphene* 2013, **1**, 78-85.

Table of Content

Title: Amorphous Carbon Nanotubes as Potent Sorbents for Removal of Phenolic Derivative Compound and Arsenic: Theoretical Support of Experimental Findings

Author: P. Bhowmik, D. Banerjee, S. Santra, D. Sen, B. Das, K. K. Chattopadhyay

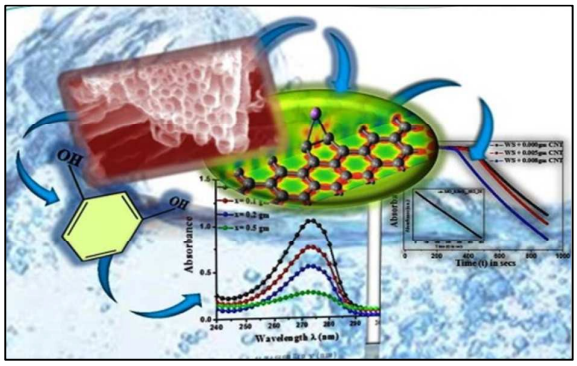

Amorphous Carbon Nanotubes can be uses as potential material for water purification